Advances in Materials Technology for Fossil Power Plants
Proceedings from the Eighth International Conference
October 11–14, 2016, Albufeira, Algarve, Portugal

J. Parker, J. Shingledecker, J. Siefert, editors

# DESIGN, CREEP PERFORMANCE AND DEFORMATION BEHAVIOR OF AN ETA-PHASE STRENGTHENED NICKEL-BASE ALLOY FOR A-USC POWER PLANT APPLICATIONS

***W.W. Milligan, P.G. Sanders and C.L. White***
*Michigan Technological University, Houghton, Michigan, USA*

***J.P. Shingledecker and D.F. Purdy***
*Electric Power Research Institute, Charlotte, North Carolina, USA*

## ABSTRACT

By utilizing computational thermodynamics in a Design of Experiments approach, it was possible to design and manufacture nickel-base superalloys that are strengthened by the eta phase ($Ni_3Ti$), and that contain no gamma prime ($Ni_3Al,Ti$). The compositions are similar to NIMONIC® 263, and should be cost-effective, and have more stable microstructures. By varying the aging temperature, the precipitates took on either cellular or Widmanstätten morphologies. The Widmanstätten-based microstructure is thermally stable at high temperatures, and was found to have superior ductility, so development efforts were focused on that microstructure. High temperature tensile test and creep test results indicated that the performance of the new alloys was competitive with NIMONIC 263. SEM and TEM microscopy were utilized to determine the deformation mechanisms during creep.

## INTRODUCTION

Wrought nickel-base alloys such as INCONEL® 740/740H and NIMONIC 263 are being considered for high-temperature high-efficiency transformational electric power generation facilities. With few exceptions, these alloys are strengthened by the gamma prime phase, designated $\gamma'$, and based on the $Ni_3Al/L1_2$ structure. During extended times at operating temperatures, other phases can form, and many of these phases are considered to be detrimental to performance. One such phase that forms in these types of alloys is the eta phase, designated $\eta$, and based on the $Ni_3Ti/D0_{24}$ structure [1].

As service conditions in advanced power generation facilities become more extreme, the use of higher performing alloys becomes necessary. However, due to the large sizes of the components, many high performance aerospace alloys are impractical for heavy section components. Further, many aerospace alloys are not suitable for welding, which is common in power generation facilities. For these reasons, alloy development efforts are currently being conducted by many research groups.

---
® NIMONIC and INCONEL are registered trademarks of the Special Metals Corporation group of companies.

In this work, an alloy development strategy was undertaken to modify NIMONIC 263, which is an existing alloy used in combustors of turbines and being considered for advanced power plants. The strategy involved thermodynamic and experimental studies aimed at eliminating the $\gamma'$ precipitates, and replacing them with $\eta$ precipitates *as the primary strengthening phase*. These alloy development studies were successful, and are fully discussed in a recent paper which contains the modeling and resultant microstructures [2]. These results will be briefly summarized here, while the remainder of this paper presents new results on mechanical behavior, deformation behavior, and fine details of the microstructures of the modified alloys.

## Alloy Development

Starting with a baseline of NIMONIC 263, a rigorous Design of Experiments study utilizing Thermo-Calc was conducted [2]. The goal was to maximize the fraction of $\eta$ precipitates after hot working and heat treatment. After studying 32 possible alloy compositions, three alloys were produced and fabricated for further study. All three alloys had reduced aluminum content (0.1% by weight vs. 0.5% in NIMONIC 263) as well as slightly increased titanium content (3% vs. 2%). Molybdenum (6% in NIMONIC 263) was completely eliminated. Based on Thermo-Calc predictions of maximizing $\eta$, Nb, W, Ta and V were added to the three alloys at levels of 0-2%. Two of these compositions were chosen for further study, and the compositions are given in Table 1 along with the nominal composition of NIMONIC 263.

*Table 1. Alloy compositions (weight percent); major changes in* ***bold***

| | HV1719A (19) | HV1720A (20) | NIMONIC 263 [3,4] |
|---|---|---|---|
| Ni | Bal | Bal | Bal |
| Co | 21 | 21 | 20 |
| Cr | 18 | 21 | 20 |
| ***Al*** | ***0.13*** | ***0.14*** | ***0.6*** |
| Fe | 0.47 | 0.48 | 0.7 |
| ***Mo*** | ***0*** | ***0*** | ***6*** |
| Mn | 0.38 | 0.42 | 0.60 |
| Si | 0.19 | 0.19 | 0.40 |
| ***Ti*** | ***2.9*** | ***2.8*** | ***2*** |
| ***Nb*** | ***1.9*** | ***1.9*** | ***0*** |
| ***W*** | ***1.9*** | ***1.9*** | ***0*** |
| ***Ta*** | ***1.9*** | ***1.1*** | ***0*** |
| ***V*** | ***0*** | ***0.85*** | ***0*** |
| C | 0.07 | 0.07 | 0.06 |

Heat treatment studies verified that both alloys contained a high fraction of $\eta$, exceeding 15% by volume, and essentially no $\gamma'$. Aging at times between 24 and 300 hours at various temperatures resulted in two distinct microstructural features. As shown in Fig. 1, alloys aged at temperatures of 1023 K (750$^{o}$C) or below exhibited a cellular microstructure similar to pearlite in steels, while alloys aged at or above 1123 K (850$^{o}$C) exhibited a Widmanstätten structure.

These microstructural trends were similar for Alloys 19 and 20 listed in Table 1, which were selected for tensile and creep testing, presented below.

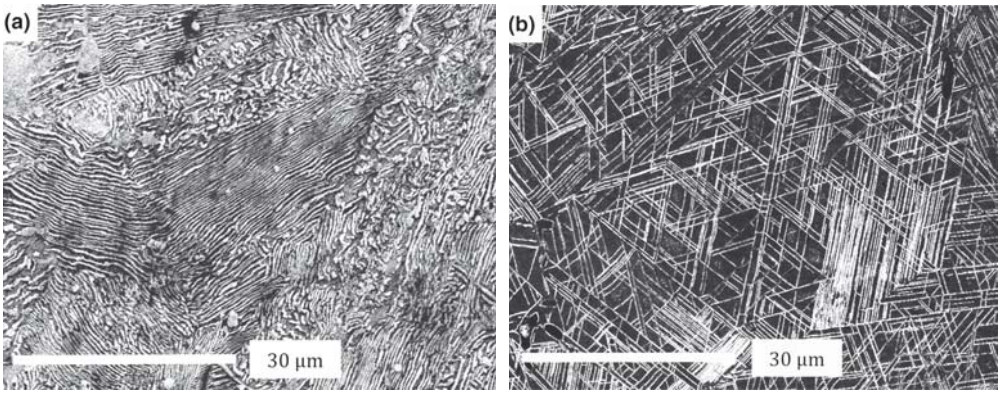


*Figure 1: Microstructures of the "V2" alloy, differing from Alloy 19 in Table 1 only be substituting 2% V for 2% Ta. (a) Cellular structure formed by aging at 1023 K. (b) Widmanstätten structure formed by aging at 1123 K [2].*

## EXPERIMENTAL PROCEDURES

Two heats of materials were produced with the compositions measured in Table 1. Heats weighing 45 kg were produced via vacuum induction melting (VIM). The heats were homogenized at 1473 K (1200$^{o}$C) for 8 hours prior to hot working. Hot working was done via rolling with frequent re-heating to produce a final plate thickness of 16 mm. Following hot-working, the plates were given a solution annealing heat treatment of 1423 K (1150$^{o}$C) for 1 hour, followed by water quenching. Two aging treatments were used: 1023 K (750$^{o}$C) to produce the cellular structure, and 1173 K (900$^{o}$C) to produce the Widmanstätten structure. Tensile test specimens were aged for 100 hours. Based on preliminary results, creep test specimens were aged at 1173 K (900$^{o}$C) for 24 hours.

High temperature tensile tests and creep rupture tests were conducted at temperatures between 1023 K (750$^{o}$C) and 1123 K (850$^{o}$C). Failed and interrupted specimens were examined by optical microscopy, as well as scanning and transmission electron microscopy. TEM foils were prepared by twin-jet electropolishing in a solution of 5% perchloric acid, 35% butyl cellusolve, and 60% methanol at 248 K (-25$^{o}$C) and 20 V. TEM microscopy was conducted on a JEOL 2010 operating at 200 kV.

## RESULTS - TENSILE BEHAVIOR

Figure 2 shows stress-strain curves for both alloys and both microstructural conditions, over a range of temperatures. Several conclusions may be drawn from Fig. 2. The cellular microstructure is substantially stronger than the Widmanstätten microstructure at lower temperatures, and slightly stronger than the Widmanstätten microstructure at 1123 K (850$^{o}$C). However, the Widmanstätten microstructure has significantly more ductility than the cellular structure. (Note that the strain axis is expanded for the Widmanstätten microstructure graph.) Finally, in all cases, Alloy 20 exhibits higher ductility than Alloy 19 despite having around the same yield strength and ultimate tensile strength.

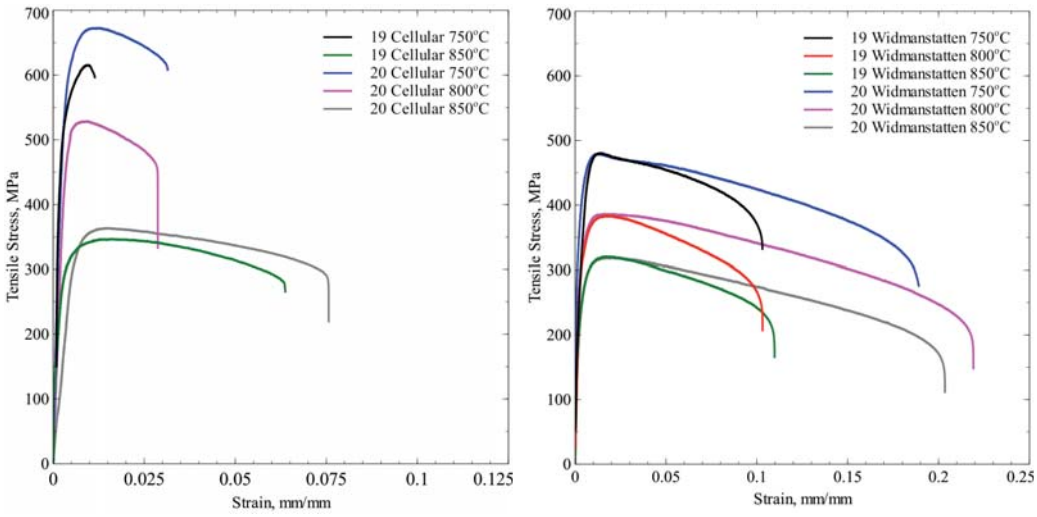


*Figure 2: High temperature tensile test behavior.*

Figure 3 compares the yield strength and ultimate tensile strength of both alloys to NIMONIC 263 handbook values. It is evident that the Widmanstätten microstructure has a yield strength that is quite similar to NIMONIC 263 at 1023 K (750°C) and 1123 K (850°C), but substantially weaker at 973 K (800°C).

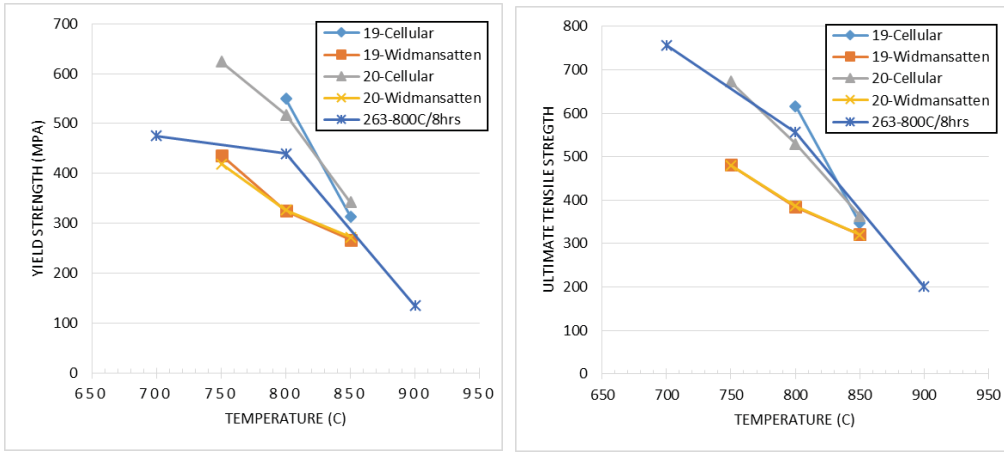


*Figure 3: Comparison of high temperature strengths to NIMONIC 263 handbook data [3-5].*

## RESULTS - CREEP BEHAVIOR

Based on the poor ductility and thermal stability of the cellular microstructure, creep testing focused exclusively on the Widmanstätten microstructure. Alloy 19 and Alloy 20 specimens were aged for 24 hours at 1173 K (900°C).

Initially, short-term creep tests were conducted on both alloys at 973-1123 K (700-850°C) with rupture times of ~20 to 140 hours. Table 2 shows the results of these short-term creep tests. The rupture lives and minimum creep rates were nearly identical for

both alloys, with most Alloy 20 tests lasting a few hours longer than Alloy 19, but with no clear trend for differences in ductility.

*Table 2: Short-term creep rupture results for Alloys 19 and 20 after aging at 1173 K for 24 hours*

| Alloy | T, K | Stress, MPa | Rupture Life, hrs. | % Elong. | % RA | Min. Creep Rate, %/hr. |
|---|---|---|---|---|---|---|
| 19 | 973 | 400 | 123.9 | 8 | 6.6 | 0.1400 |
| 19 | 1023 | 300 | 74.6 | 11 | 9.4 | 0.0303 |
| 19 | 1073 | 250 | 21.1 | 11.2 | 12.6 | 0.1670 |
| 19 | 1123 | 150 | 34.6 | 9.6 | 15.2 | 0.1150 |
| 20 | 973 | 400 | 135.4 | 9.6 | 10.1 | 0.0138 |
| 20 | 1023 | 300 | 83.2 | 9.8 | 15.1 | 0.0294 |
| 20 | 1073 | 250 | 19.9 | 11.8 | 11 | 0.1800 |
| 20 | 1123 | 150 | 48.9 | 9.1 | 8.1 | 0.0750 |

Based on these results, the longer-term creep rupture testing focused on Alloy 20. The decision to focus on Alloy 20 was made on the basis of good tensile ductility in the overaged condition, good microstructural stability, equivalent creep behavior to alloy 19, and what was judged to be a more favorable composition in terms of alloy cost since Ta is more expensive than V. Currently, long-term testing has surpassed 5,000 hours for the longest duration tests. Figure 4 is a Larson Miller Parameter Plot (LMP) comparing the time to rupture data for all the current completed, interrupted, and ongoing tests on alloy 20 in comparison to average alloy 263 behavior and the behavior of a similar alloy, INCONEL 740/740H. Both alloy 263 and 740 are $\gamma'$ strengthened alloys. Inspection of the data clearly show that the creep rupture strength of alloy 20, which has no $\gamma'$, is nearly equivalent to that of Alloy 263.

Based on these tensile and creep results, the alloy development strategy appears to have potential. Without optimizing microstructures, the tensile and creep behavior of Alloy 20 are competitive with NIMONIC 263. Additionally, the alloy cost increases from alloy additions are expected to be modest (1% Ti, Ta and V; 2% Nb and W.) The alloys may be even less expensive, since 6% Mo was eliminated.

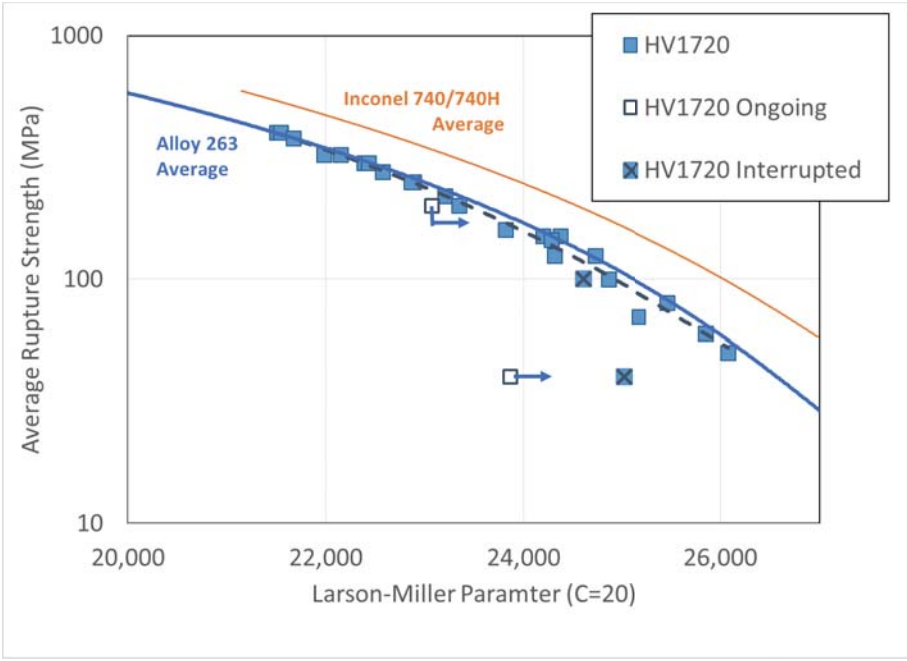


*Figure 4. LMP plot of alloy 20 (HV1720) data (aged at 1173 K for 24 hours) compared to typical behavior for Alloy 263 [3-5] and INCONEL 740/740H [6].*

## RESULTS - MICROSTRUCTURE AND DEFORMATION BEHAVIOR

A study of the microstructure and deformation behavior of Alloy 20 after creep and high temperature tensile testing is currently in progress. Preliminary results are reported below. These results were obtained by studying an interrupted creep specimen that had been tested at 1073 K (800$^{o}$C) under a stress of 100 MPa for 840 hours. The specimen experienced 1.6% plastic strain, and had reached approximately 60% of its expected creep life.

The undeformed microstructure was examined by TEM samples taken from the grip end of the creep specimen. Figure 5(a) shows a low magnification TEM micrograph illustrating the Widmanstätten microstructure. Figure 5(b) shows a higher magnification image of the precipitate interface structure. An $\eta/\gamma$ interface is contained in the foil, and one may observe an array of interfacial dislocations in this interface. This indicates that the interface is semi-coherent. Such arrays have been observed in NIMONIC 263 $\eta/\gamma$ phase interfaces after extended heat treatment [7].

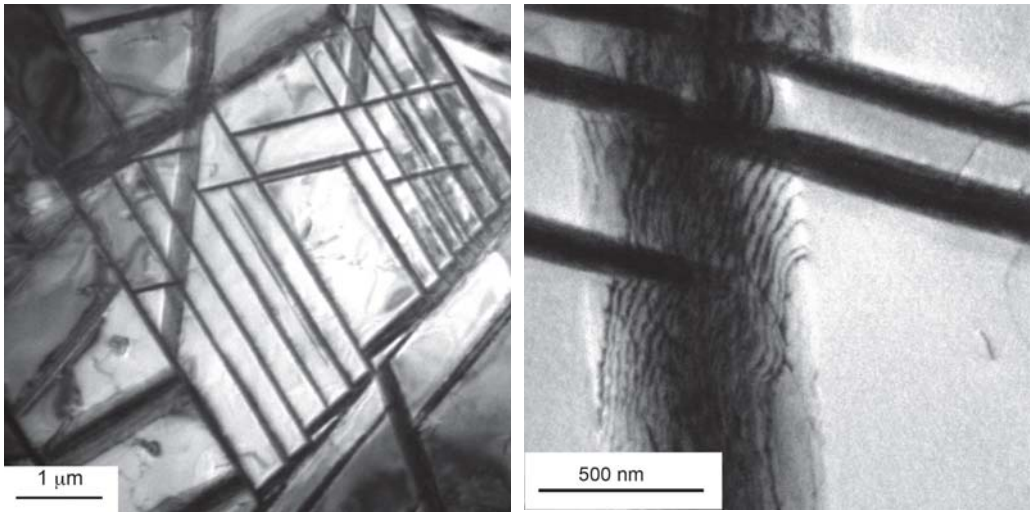


(a) (b)

*Figure 5: TEM microstructure of Alloy 20 in the undeformed section (grip end) of the creep bar after 840 hours at 1073 K. (a) Low magnification. The $\eta$ plates are thin and have different apparent thicknesses due to thin foil projection effects. That is, plates perpendicular to the plane of the foil have a small projected width, while plates nearly in the plane of the foil have a large projected width. (b) Higher magnification. The three black bands running horizontally in the photo are $\eta$ plates that are steeply inclined to the plane of the photo, nearly parallel to the electron beam. The large feature running vertically that takes up most of the left hand side of the photo is an $\eta$ plate that is almost completely in the plane of the photo, virtually perpendicular to the electron beam.*

Figure 6 shows several other features that were very common in the microstructure. There are matrix dislocations in the $\gamma$ phase that are connected to the interfaces. In Fig. 6(a), a dislocation node connecting the interfacial dislocation network to a matrix dislocation (arrow) is clearly evident. In Fig. 6(b), there are four parallel $\eta$ phase plates steeply inclined to the plane of the micrograph, and matrix dislocations connected on both sides to the $\eta/\gamma$ interface are clearly visible. These matrix dislocations appear to be bowing outward and anchored by the interface, perhaps under stress during hot working or thermal stress during heat treatment.

Tensile and creep specimens are currently being studied after deformation by TEM. Preliminary results from the Alloy 20 creep specimen that was interrupted after 1.6% plastic strain, under a stress of 100 MPa at 1073 K (800$^{o}$C), are presented below.

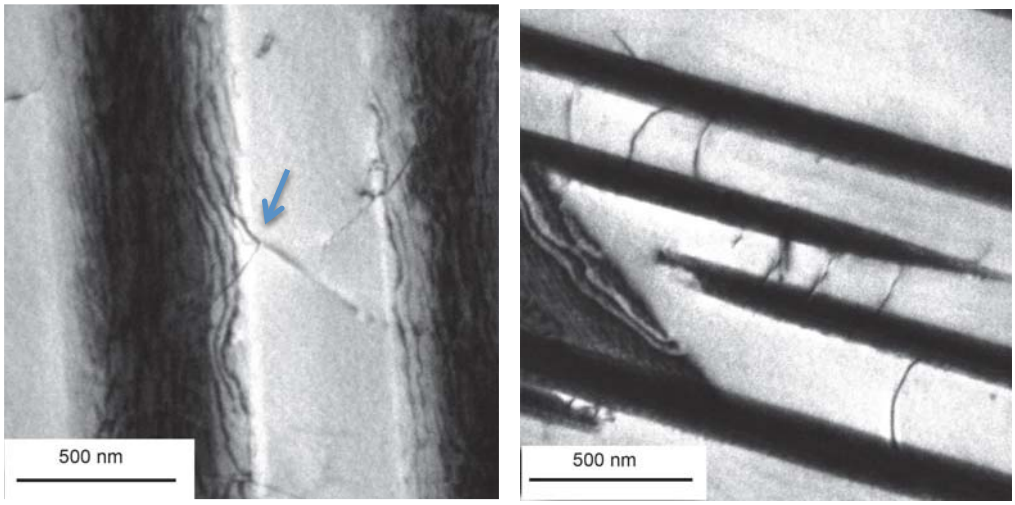


(a) (b)

*Figure 6: Interfacial and matrix dislocations in the undeformed Alloy 20. (a) Matrix dislocation connected to interfacial array at a node (arrow). (b) Matrix dislocations connected to interfaces on both sides, apparently bowing out under stress during processing or heat treatment. The large dark feature on the left-hand side of the micrograph is an $\eta$ plate that is nearly perpendicular to the electron beam, in the plane of the foil.*

In Fig. 7(a), a matrix dislocation appears to be bowing out into the matrix from the interfacial network (arrow). The arrow in Fig. 7(b) marks another matrix dislocation bowing out from the interfacial network. There are a number of other matrix dislocations in both figures which are also attached on at least one side to an $\eta$ precipitate, and probably are attached on the other side, but were truncated by the foil surface. These images suggest that the interfacial dislocation network is a potent source of matrix dislocations, which may aid deformation and explain the ductility of these alloys.

Figure 8 shows additional features commonly observed during creep deformation at 1073 K. Figure 8(a) shows evidence of dislocations bowing out and anchored at the interface, similar to the undeformed specimen of Fig. 6(b). Figure 8(b) shows several areas containing parallel dislocations gliding in the matrix (arrows), which are basically small slip bands that probably initiated in an $\eta/\gamma$ phase boundary sources.

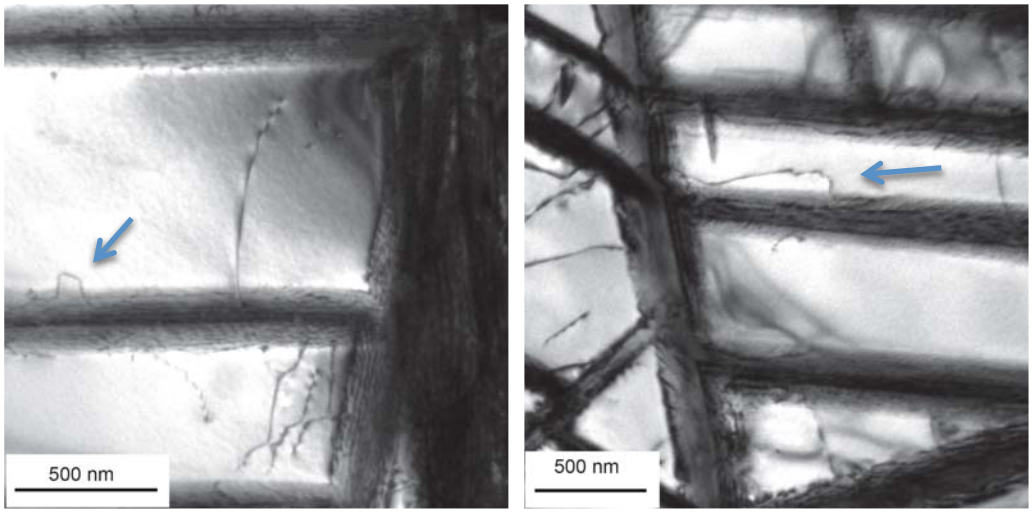


(a) (b)

*Figure 7: Interfacial dislocation sources (arrows) activated during creep of Alloy 20 at 1073 K. Please see text for discussion.*

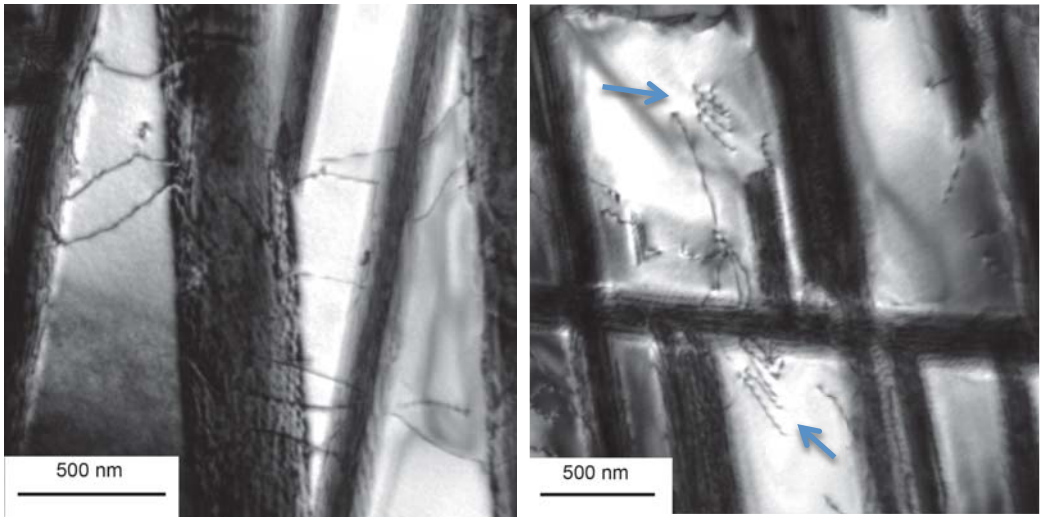


(a) (b)

*Figure 8: Deformation observed in Alloy 20 crept at 1073 K. (a) Dislocation bowing in the matrix, anchored at the precipitate interface. (b) Parallel dislocations (slip band, arrowed) in the matrix.*

Importantly, *no evidence of $\eta$ precipitate shearing was observed in this specimen.* The deformation all appeared to be in the matrix and at the interface. 1073 K is a fairly high temperature for the nickel-base matrix, so it is expected that dislocation climb and cross slip, along with a mobile interfacial dislocation array, could accommodate the deformation at this relatively small strain (1.6%). It is also possible that some shearing of the $\eta$ platelets occurred, but that the shear offsets were too small to be detectable.

At higher strains and/or lower temperatures, we expect that volume fraction and compatibility issues will require the $\eta$ plates to deform, or else little ductility would be expected. Since reasonable ductility is observed in these alloys even at room temperature, the $\eta$ platelets must be capable of deformation, and TEM studies are currently underway to identify these deformation mechanisms. Figure 9 shows an SEM micrograph of an Alloy 20 specimen that was crept to failure at 1123 K (850$^{o}$C) under a stress of 150 MPa. Rupture life was 49 hours with 9% elongation. In this micrograph, there is clear evidence of significant warping of the $\eta$ plates, especially near the grain boundaries. Further work is in progress to determine how these plates deformed, and to determine tensile and creep deformation mechanisms for each temperature.

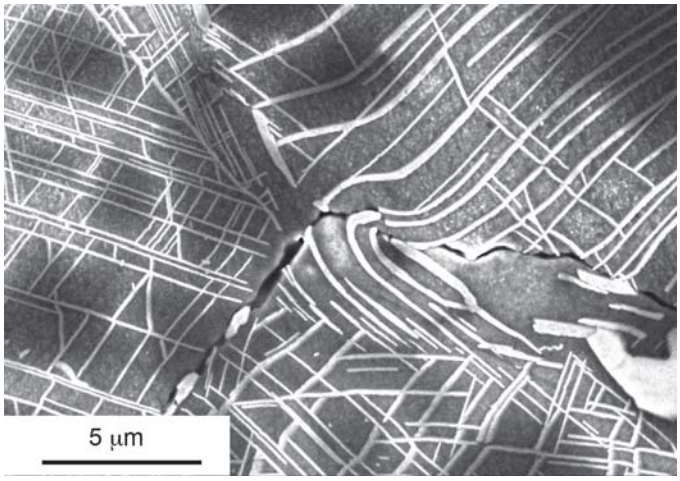


*Figure 9: SEM micrograph of Alloy 20 after creep rupture, 1123 K (850$^{o}$C), showing substantial deformation (curvature) of the $\eta$ plates, which were all straight before creep.*

## CONCLUSIONS

Using computational thermodynamic modeling in a Design of Experiments approach, nickel-base superalloys that contain only $\eta$ phase precipitates, and no $\gamma'$ have been designed. The compositions are relatively close to NIMONIC 263, and should be cost-effective.

Heat treatment produced microstructures that were either cellular (low temperature aging) or Widmanstätten (high temperature aging, above about 1123 K). The Widmanstätten microstructure is thermally stable at elevated temperatures, and has excellent ductility.

Tensile and creep test results indicated that the high temperature mechanical properties of the Widmanstätten-microstructure alloys were competitive with NIMONIC 263, and thus suggest that further alloy development and microstructural optimization could be pursued, especially with a goal of increasing strength.

TEM studies found an interfacial dislocation array at the $\eta/\gamma$ precipitate interfaces. These arrays were potent sources for matrix dislocations during deformation. Analysis of a specimen that had been crept at 1073 K to 1.6% creep strain revealed substantial deformation in the matrix, but no evidence of $\eta$ phase shearing. SEM analysis of a

specimen crept to failure at 1123 K revealed substantial deformation of the plate-shaped $\eta$ phase precipitates.

## ACKNOWLEDGMENTS

Michigan Tech would like to thank Matthew Wong and Janine Erickson for experimental assistance, EPRI's Technology Innovation Strategic Program on Materials for financial assistance in support of this research, and alloy processing by Special Metals.

## REFERENCES

[1] Shingledecker, J.P. and Pharr, G.M., "The role of eta phase formation on the creep strength and ductility of INCONEL alloy 740 at 1023 K (750 C)," *Metall. Mater. Trans. A,* Vol. 43A (2012), pp. 1902-1910.

[2] Wong, M.J., Sanders, P.G., Shingledecker, J.P. and White, C.L., "Design of an Eta-Phase Precipitation-Hardenable Nickel-Based Alloy with the Potential for Improved Creep Strength Above 1023 K (750° C)," *Metall. Mater. Trans. A,* Vol. 46A (2015), pp. 2947-2955.

[3] Vendor dataset: NIMONIC 263, SMC-054, Special Metals Corporation (2004). Available online at www.specialmetals.com

[4] Vendor dataset: Haynes 263 Alloy, H-3047D, Haynes International, Inc. (2000). Available online at www.haynesintl.com.

[5] Yamamoto, M., Shingledecker, J., Boehlert, C., Ogata, T. and Santella, M., "Microscopic Evaluation of Creep-fatigue Interaction in a Nickel-based Superalloy," *Proceedings: Creep & Fracture in High Temperature Components, 2nd ECCC Creep Conference,* Zurich, Switzerland, April 2009, DEStech Publications, Inc., pp. 1205-1215.

[6] Shingledecker, J.P., Evans, N.D. and Phar, G.M., "Influences of Composition and Grain Size on Creep-Rupture Behavior of INCONEL® Alloy 740," *Materials Science and Engineering A., Vol.* 578 (2013), pp. 277-286.

[7] Zhao, J.-C., Ravikumar, V. and Beltran, A.M., "Phase Precipitation and Phase Stability in NIMONIC 263," *Metall. Mater. Trans. A,* Vol. 32A (2001), pp. 1271-1282.